GENERATING LOW-RCS SPARSE WIRE GRID ANTENNAS USING NEW MODIFICATION OF OPTIMAL CURRENT GRID APPROXIMATION

DOI: 10.36724/2072-8735-2026-20-8-54-65

Manuscript received 04 April 2026;
Accepted 12 July 2026

Xuan Ba Trinh,
Tomsk State University of Control Systems and Radioelectronics (TUSUR), Tomsk, Russia, ***xuanba6420@gmail.com***

Talgat R. Gazizov,
Tomsk State University of Control Systems and Radioelectronics (TUSUR), Tomsk, Russia, ***talgat.r.gazizov@tusur.ru***

Keywords: *optimal current grid approximation, method of moments, wire grid, sparse antenna, radar cross section*

Simultaneously reducing the mass and radar cross section (RCS) of an antenna is a design challenge that has attracted considerable attention in recent research. This study proposes the Low-RCS Optimal Current Grid Approximation (L-RCS-OCGA) aimed at simultaneously reducing both the mass and the RCS while preserving the fundamental radiation characteristics. The proposed approach sparsifies a wire grid (WG) antenna by eliminating wires that contribute weakly to the radiation field and strongly to the backscattered field, and then restores connectivity among disconnected components by reconnecting through wires with the smallest contribution to the scattered field. This represents the modification made for the first time in the OCGA family to incorporate scattering awareness into both the wire-elimination and reconnection steps. L-RCS-OCGA was validated by both simulation and measurement on a WG trihedral corner reflector antenna operating at 6 GHz, with the monostatic RCS examined over the 5-8 GHz band for both -polarized and right-hand circularly polarized (RHCP) incident waves. The representative sparse antenna is 2.12 times lighter than the original one, with an average RCS reduction at boresight of 6.73 dB in simulation, 8.16 dB in measurement for -polarized incidence and 10.3 dB in simulation for the total RHCP component, while the fundamental radiation characteristics remain close to those of the original antenna. L-RCS-OCGA, therefore, achieves simultaneous mass and RCS reduction, making it particularly suitable for platforms with stringent payload constraints.

Information about authors:

Xuan Ba Trinh, P*h.D. Student, TUSUR, Tomsk, Russia. ORCID: 0009-0000-5711-5878*

Talgat R. Gazizov, *Doctor of Engineering Sciences, Professor, Head of Department, TUSUR, Tomsk, Russia. ORCID: 0009-0000-6287-1117*

Для цитирования:
Чинь С. Б., Газизов Т. Р. Создание разреженных проводно-сеточных антенн с уменьшенной ЭПР, используя новую модификацию аппроксимации оптимальной токовой сеткой // T-Comm: Телекоммуникации и транспорт. 2026. Том 20. №8. С. 54-65.

For citation:
X. B. Trinh, T. R. Gazizov, "Generating low-RCS sparse wire grid antennas using new modification of optimal current grid approximation," *T-Comm*, 2026, vol. 20, no. 8, pp. 54-65.

1. Introduction

Antennas play an essential role in many modern fields, ranging from wearable smart devices [1], medical Internet of Things devices [2], to satellite communications [3]. Along with this diversity of applications, the requirements imposed on antennas have become increasingly stringent, particularly in terms of mass and scattering behavior. On the one hand, antenna mass needs to be reduced in order to be compatible with systems that are limited in payload and installation space. On the other hand, the antenna must exhibit a low radar cross section (RCS) to enhance the stealth performance of the overall system [4, 5]. Meeting these two requirements simultaneously is a non-trivial design challenge.

A number of recent studies have proposed approaches for reducing the antenna RCS based on metasurfaces [6-8], frequency-selective surfaces [9, 10], radar-absorbing materials [11], and characteristic mode analysis [12, 13], and have achieved notable performance. However, these approaches typically require the integration of auxiliary structures or additional design steps, which leads to an increase in the system complexity and overall mass. In several cases, the additional structures involved also degrade the antenna radiation performance [11, 14]. Therefore, an approach that can reduce the RCS without introducing additional materials or auxiliary structures would offer a clear practical advantage, especially for platforms with stringent mass constraints.

A promising candidate in this direction is the sparsification of wire grid (WG) structures by means of the optimal current grid approximation (OCGA), which has been developed in recent studies [15-19]. OCGA relies on the method of moments (MoM) [20] to determine the current distribution over the wires, and then removes the wires that carry small currents, since they contribute insignificantly to the radiation characteristics. Existing studies have demonstrated that OCGA can significantly reduce the mass of the WG antenna while preserving its main radiation characteristics. However, the wire-elimination criterion adopted in those studies relies only on the contribution of each wire to the radiation, and does not consider its contribution to the scattered field of the antenna. As a result, the potential of OCGA-based sparsification for reducing the RCS has not yet been systematically exploited and assessed.

In addition, an issue that arises when applying OCGA is that the resulting sparse structure may be split into separate, disconnected components, which complicates fabrication. To address this issue, several OCGA modifications have been proposed in the direction of restoring some of the previously eliminated wires in order to reconnect these separate components; they include near-connecting OCGA (NCOCGA) [16] and maximum current-based OCGA (MCOCGA) [17]. In these modifications, the wires to be restored are selected based on the criterion of the number of wires required for the reconnection, or on the magnitude of the currents on the wires associated with the radiation, without considering their contribution to the scattered field.

In order to simultaneously address the two gaps identified above, this work proposes a sparsification approach for WG antennas, named Low-RCS Optimal Current Grid Approximation (L-RCS-OCGA), which allows the mass and the RCS of the antenna to be simultaneously reduced while preserving its basic radiation characteristics. The approach consists of the following two components. First, the wire-elimination criterion is extended to account for the contribution of each wire to the scattered field, thereby enabling a deliberate RCS reduction. Second, the reconnection mechanism gives priority to wires with smaller contributions to the scattered field, ensuring fabrication feasibility without compromising the RCS reduction. The effectiveness of L-RCS-OCGA was verified through simulation and measurement on a triangular trihedral corner reflector (TCR) WG antenna [21, 22] operating at 6 GHz, with the monostatic RCS examined over the 5-8 GHz frequency band for both linearly and circularly polarized incident waves.

The remainder of this article is organized as follows. Section 2 elaborates on the proposed L-RCS-OCGA approach. Section 3 applies the approach to a TCR WG antenna and presents the simulation results. Section 4 reports the experimental results obtained on the fabricated prototypes. Section 5 discusses the implications and limitations of the proposed approach, and Section 6 concludes the work.

2. Low-RCS Optimal Current Grid Approximation

The main idea of the L-RCS-OCGA approach consists in the following. Applying OCGA eliminates the wires that have little influence on the radiation field, thereby reducing the mass of the antenna while preserving its basic radiation characteristics. In this work, we generate a set of different sparse antennas and choose two, hereinafter called the Base and Reference antennas. Then, we sparsify the Base antenna by eliminating the wires that have a strong influence on the scattered field of this antenna, thereby simultaneously reducing both its RCS and mass. The degree of degradation of the radiation characteristics is controlled by the Reference antenna. After this sparsification, disconnected wire components are reconnected by means of a reconnection mechanism that gives priority to the wires with smaller contributions to the scattered field, without compromising the RCS reduction. The L-RCS-OCGA approach consists of three steps, as illustrated in Fig. 1.

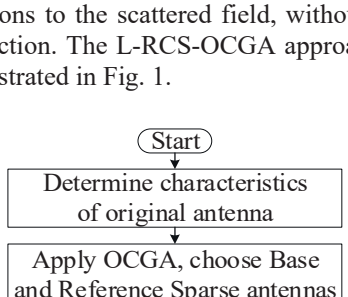


Fig. 1. Overall L-RCS-OCGA flowchart

In step 1, the antenna is analyzed by MoM [20] with pulse basis functions. Each wire of the WG is represented by a segment, while the excitation elements requiring a more detailed description of the current distribution can be divided into multiple segments. For the radiation problem, the excitation vector **v** has only one non-zero entry, corresponding to a 1 V voltage applied at the excitation segment. The MoM system of equations $\mathbf{Zi} = \mathbf{v}$ is then solved, where **Z** is the impedance matrix and **i** is the unknown vector, whose entries correspond to the currents on the individual segments. From this solution, the basic character-

istics of the antenna are determined, including the reflection coefficient and radiation pattern.

In step 2, OCGA is applied to eliminate the wires with small currents, as they contribute insignificantly to the antenna radiation characteristics, thereby generating a set of sparse antennas with different sparsification levels. The specific procedure follows [17], where the MoM system of equations is first solved for the radiation problem at a frequency *f*. The current magnitudes obtained on the wires are normalized with respect to the maximum or the average value, and the normalized result is denoted by $|I_n|$, where n is the wire index. Each $|I_n|$ value is then compared with a predefined threshold, called the Grid Element Elimination Tolerance (GEET), expressed in percent. A wire with $|I_n|$ smaller than GEET is considered a wire with a small current and is added to the Eliminated Wires List, while the remaining wires are added to the Remaining Wires List. Previous studies [15, 17, 19] have shown that eliminating wires in this way significantly reduces the antenna mass while keeping the radiation pattern unchanged. By varying GEET, a number of different sparse antennas can be obtained. A larger GEET produces a lighter structure, but may degrade the radiation characteristics.

From the set of sparse antennas obtained, the Base and Reference antennas are chosen. The Base antenna is the structure that achieves a substantial mass reduction while its radiation characteristics remain close to those of the original antenna. The Reference antenna is the structure with the highest level of sparsification that is still acceptable, in the sense that any further sparsification would significantly degrade the radiation characteristics. To ensure consistency, both the Base and Reference antennas are generated by OCGA with the same type of current normalization, so that the set of wires of the Reference antenna is a subset of the set of wires of the Base antenna. The set of wires that are present in the Base antenna but not in the Reference antenna is called the Candidate set, whose number of elements is denoted by *N*.

In step 3, we further sparsify the Base antenna by eliminating the wires that significantly influence the scattered field, and then restores the connection between the disconnected components in order to ensure fabrication feasibility. To evaluate the contribution of each wire to the scattered field, the MoM is formulated for the scattering problem. In this state, the antenna is not excited by its internal source, but by an incident plane wave, and the excitation segment is loaded with 50 Ω. In this work, the incident plane wave is described by the spatial phasor convention $e^{+j\mathbf{kr}}$ with θ-polarization (θ-pol) (described in detail in Section 3); here, **k** is the wave vector pointing in the direction of propagation ($|\mathbf{k}| = 2\pi/\lambda$ where λ is the wavelength), and **r** is the position vector.

The plane-wave excitation is applied successively from a set of incidence directions (θ, φ) at a frequency *f*, which is chosen to evaluate the contribution of the wires to the scattered field. Based on this, two non-negative scalar metrics (*M* and *J*) are defined for each wire, each characterizing the contribution of that wire to the scattered field. The metric *M* is determined on the original antenna and is the average of the current magnitude on the corresponding wire over the set of all considered incident directions.

The metric *J* is determined in the same way, but on the Base sparse antenna. The two metrics are used for two different purposes: *J* is used to further eliminate the wires of the Base that have a strong contribution to the scattered field, while *M* is used as a priority criterion in the reconnection. The two processes of wire elimination and reconnection are illustrated in detail in Fig. 2.

For the wire-elimination process, *J* for each wire is normalized with respect to the maximum or the average value, and is then compared with a threshold, called the Grid Element Elimination Tolerance for RCS ($GEET_{RCS}$). A wire with *J* greater than $GEET_{RCS}$ and also belongs to the Candidate set, is moved from the Remaining Wires List of the Base antenna to its Eliminated Wires List. Restricting the elimination to the Candidate set ensures that this additional sparsification does not push the structure beyond the Reference antenna, so that the radiation characteristics are maintained at a controlled level. From a physical point of view, the scattered field of the structure is produced by the currents on its wires under the incident plane wave, so that the wires with larger *J* contribute more strongly to the RCS [18]. Eliminating these wires directly suppresses the strongest scattering sources within the permitted limits. By varying $GEET_{RCS}$, a number of different sparse antennas can be obtained at the output of this step.

After this sparsification, the resulting structure may contain disconnected wire components that are not linked to one another. To handle this issue, the wires in the Remaining Wires List of the sparse structure, obtained after the RCS reduction step, are classified into two subsets following a procedure similar to that in [17]. The first subset, called the Connected Wires List, contains the main structure, defined as the component that includes the excitation segment. The second subset, called the Free Wires List, consists of *K* free-wire components; each of these components is a set of wires connected to one another but not yet connected to the main structure. In order to apply a shortest-path algorithm, in this work, the structure is represented by an undirected graph derived from the original antenna where each wire of the WG is an edge, and each junction between wires is a vertex. On this graph, the multi-source Dijkstra algorithm [23] is applied to find a reconnection path from a free-wire component back to the main structure with the minimum number of restored wires. When several paths share the same minimum number of wires, the selected path is the one with the smallest total *M* (the sum of the average per-wire currents under plane-wave excitation, defined earlier), that is, the path consisting of wires that contribute the least to the scattered field. The selected wires are then moved from the Eliminated Wires List to the Connected Wires List. This procedure is repeated for each free-wire component until the Free Wires List is empty. Giving priority to wires with small *M* during the reconnection ensures that the connection mechanism does not compromise the RCS reduction achieved in the elimination step. As a result, the L-RCS-OCGA procedure is expected to simultaneously achieve the three objectives: to reduce mass, to reduce RCS, and to preserve the radiation characteristics of the antenna at an acceptable level.

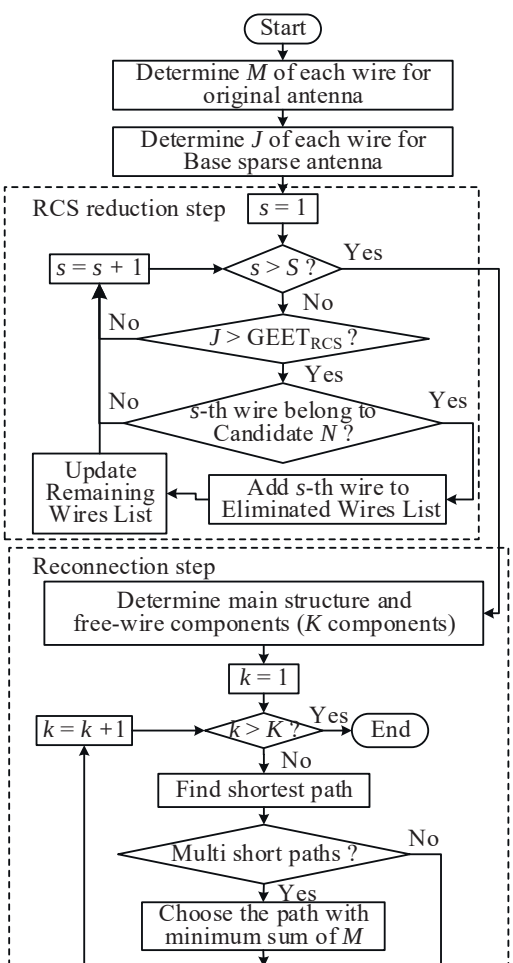
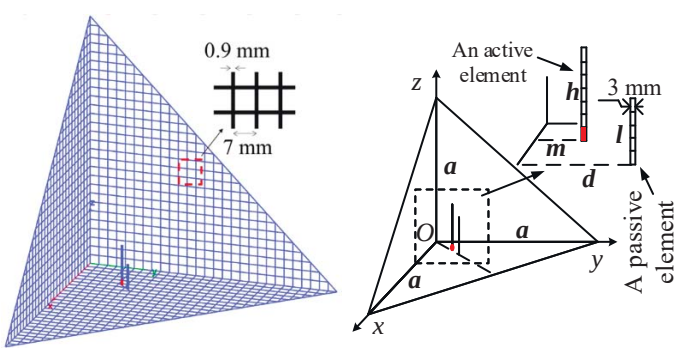


Fig. 2. Detailed flowchart of the low-RCS sparse antenna generation step

3. L-RCS-OCGA for triangular trihedral corner reflector WG antenna

To validate L-RCS-OCGA, the proposed approach was applied to a TCR WG antenna operating at 6 GHz [21, 22]. We chose the TCR because it exhibits a large monostatic RCS (MRCS) that is strongly concentrated at boresight (φ = 45° and θ ≈ 55°) [24-26], which makes it a particularly demanding test case for RCS reduction. The original antenna consisted of three faces, each of which was an isosceles right triangle with a leg length a = 196 mm (Fig. 3a). The structure was modeled as a WG with a mesh size of 7 mm (≈ λ/8 at 6 GHz) and a wire diameter of 0.9 mm. The antenna was excited by an active element of height h = 32 mm, a vertical wire divided into 7 equal segments. The segment connecting the active element to the bottom face (marked in red in Fig. 3b) served as a source gap, i.e., an excitation segment corresponding to the non-zero entry of the excitation vector **v** with a value of 1 V. A passive element of height l = 20 mm, divided into 5 segments, was used for matching the impedance to 50 Ω [22]. Both elements had a diameter of 3 mm, were oriented parallel to the Oz axis, and were placed on the bisector of the bottom face. Their perpendicular distances from each side edge were m = 38.5 mm for the active element and d = 45.5 mm for the passive element (Fig. 3b).

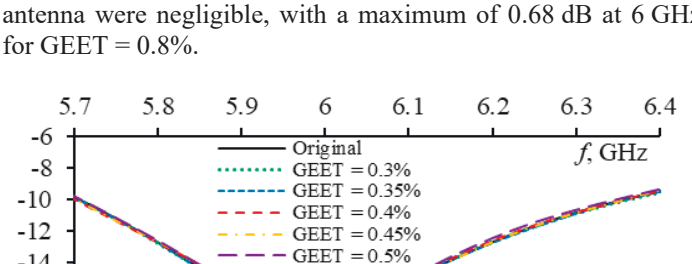


(a) (b)

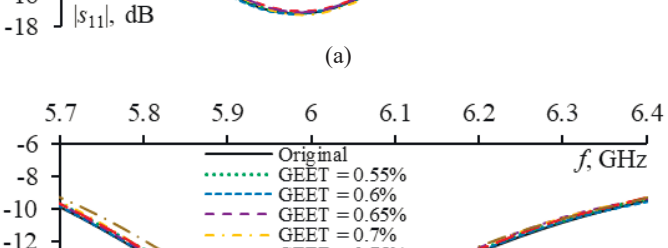
Fig. 3. TCR WG antenna (a), antenna geometry parameters (b)

OCGA was applied to the TCR WG antenna at 6 GHz, based on the MoM implemented in MATLAB. The current magnitudes on the wires were normalized with respect to the maximum, and GEET was investigated in the range from 0.3% to 0.8% with a 0.05% step. The simulation results are presented in Fig. 4 and Table 1.

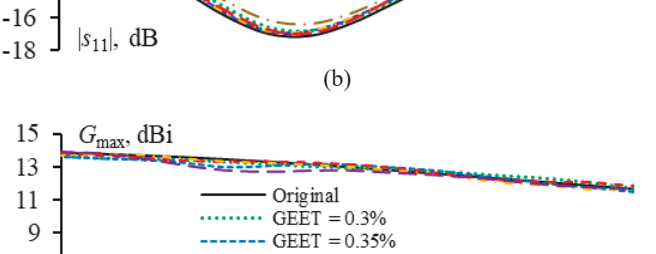
The original structure exhibited resonance at 6 GHz with a reflection coefficient magnitude $|s_{11}| \approx -17$ dB. All sparse antennas yielded $|s_{11}|$ responses consistent with those of the original antenna and remaining below –10 dB across the 5.75–6.35 GHz band (Fig. 4a and b). The deviations from the $|s_{11}|$ of the original antenna were negligible, with a maximum of 0.68 dB at 6 GHz for GEET = 0.8%.



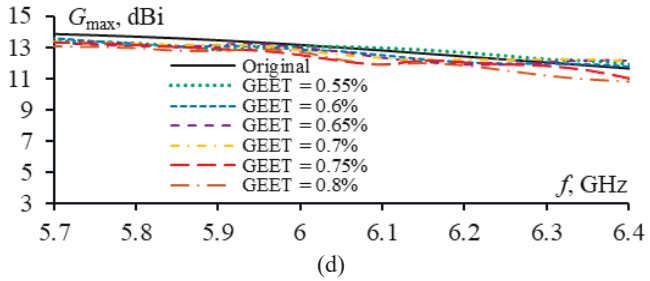
(a)



(b)

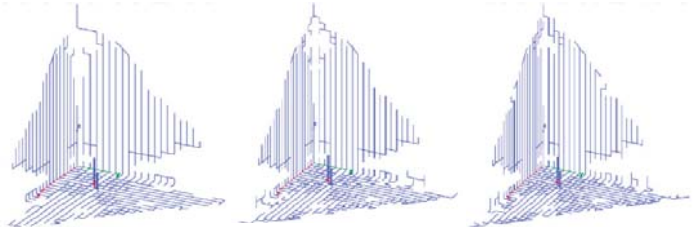


(c)



(d)

Fig. 4. Frequency dependences of the simulated $|s_{11}|$ (a, b) and G_{max} (c, d) for the original and sparse antennas after OCGA



(a) (b) (c)

Fig. 5. Sparse antennas after L-RCS-OCGA with $GEET_{RCS}$ = 10% (a), 15% (b), and 20% (c)

For the radiation characteristics, the maximum gain G_{max} of the original structure reached 13.18 dBi at the resonant frequency (Fig. 4c and d). For GEET in the 0.3–0.5% range, the G_{max} of the sparse antennas closely followed that of the original, with a maximum deviation of approximately 0.41 dBi (GEET = 0.5%) and a minimum of 0.02 dBi (GEET = 0.45%) at 6 GHz. Notably, for GEET = 0.4%, $G_{max} \approx$ 13.29 dBi at 6 GHz, slightly exceeding the original value, while maintaining very low variation across the 5.75–6.35 GHz band. As GEET increased further, the degradation of G_{max} became more pronounced. Specifically, for GEET values of 0.75% and 0.8%, the G_{max} decreased throughout the entire operating frequency band. This degradation was likely due to the elimination of a large number of wires, which reduced the effective surface density of the WG and allowed a portion of the radiated energy to leak through the structure. Nevertheless, for GEET = 0.75%, the G_{max} remained at an acceptable level, with a maximum reduction of only about 0.95 dBi at 6.1 GHz. In contrast, GEET = 0.8% caused a significantly more pronounced degradation in the high-frequency region of 6.05–6.35 GHz. To quantitatively compare the levels of sparsification, the mass reduction factor (MRF) is defined as the ratio of the mass of the original WG antenna to that of the corresponding sparse antenna and is summarized in Table 1.

Table 1

MRF of the sparse antennas

GEET,%	0.3	0.35	0.4	0.45	0.5	0.55	0.6	0.65	0.7	0.75	0.8
MRF	1.63	1.72	1.83	1.94	2.04	2.17	2.28	2.41	2.50	2.65	2.82

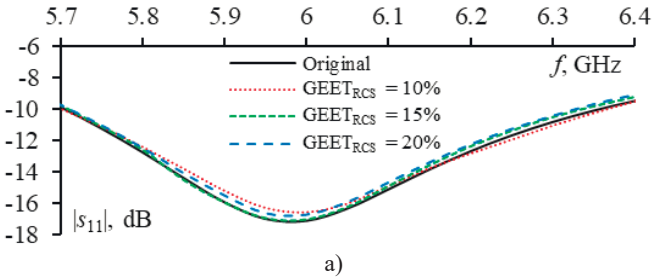
Following the definitions of the Base and Reference antennas given in Section 2, GEET = 0.4% (MRF = 1.83) was chosen as the Base sparse antenna, since it achieved substantial mass reduction while its radiation characteristics remained close to those of the original antenna. The structure with GEET = 0.75% (MRF = 2.65) was chosen as the Reference sparse antenna, since it represented the highest sparsification level for which $|s_{11}|$ and G_{max} were still acceptable. Beyond this point, as observed for GEET = 0.8%, the radiation performance was significantly degraded in the 6.05–6.35 GHz range.

L-RCS-OCGA was then applied to the Base sparse antenna at f = 6 GHz. The set of incident directions considered for the computation lay in the space in front of the TCR antenna, with θ and φ varying from 0° to 90° in 1° steps. The procedure was carried out for three values of $GEET_{RCS}$ = 10, 15, and 20%, after which the free-wire components were reconnected to the main structure (Fig. 5).

The $|s_{11}|$ of the sparse antennas closely followed that of the original antenna over the entire operating band (Fig. 6a). The most noticeable difference appeared at the resonant frequency, with a maximum deviation of approximately 0.5 dB for $GEET_{RCS}$ = 10%. These deviations were small, indicating that L-RCS-OCGA did not significantly affect the impedance matching of the antenna.

The G_{max} of the sparse antennas was also in good agreement with that of the original antenna (Fig. 6b). However, as some additional wires were eliminated, G_{max} exhibited a reduction relative to the original. At the resonant frequency of 6 GHz, this reduction was approximately 0.65, 0.18, and 0.07 dBi for $GEET_{RCS}$ = 10, 15, and 20%, respectively (Table 2). All of these values remained within a tolerable range for practical applications. It should be noted that $GEET_{RCS}$ behaved in the opposite manner compared with the GEET introduced in Step 2. A larger GEET eliminated more wires (those with $|I_n|$ below the threshold) and yielded a sparser structure, whereas a larger $GEET_{RCS}$ eliminated fewer wires (those with J above the threshold) and yielded a less sparse one.

As for the radiation patterns (RPs), the main beams of the sparse antennas remained in good agreement with the main beam of the original antenna in both the φ = 45° and θ = 33° planes (Fig. 6c and d). However, the side-lobe level (SLL) showed an increasing trend, primarily in the angular range of 180-240° in both planes. This change can be attributed to the modification of the current distribution and the loss of phase coherence in the radiated field when some wires were eliminated. The additional elimination of wires from the Base sparse antenna also made the resulting structures lighter, with MRF = 2.47, 2.25, and 2.12 for $GEET_{RCS}$ = 10, 15, and 20%, respectively. Thus, after applying L-RCS-OCGA, the mass of the original antenna was substantially reduced, while the basic radiation characteristics were maintained at an acceptable level.



a)

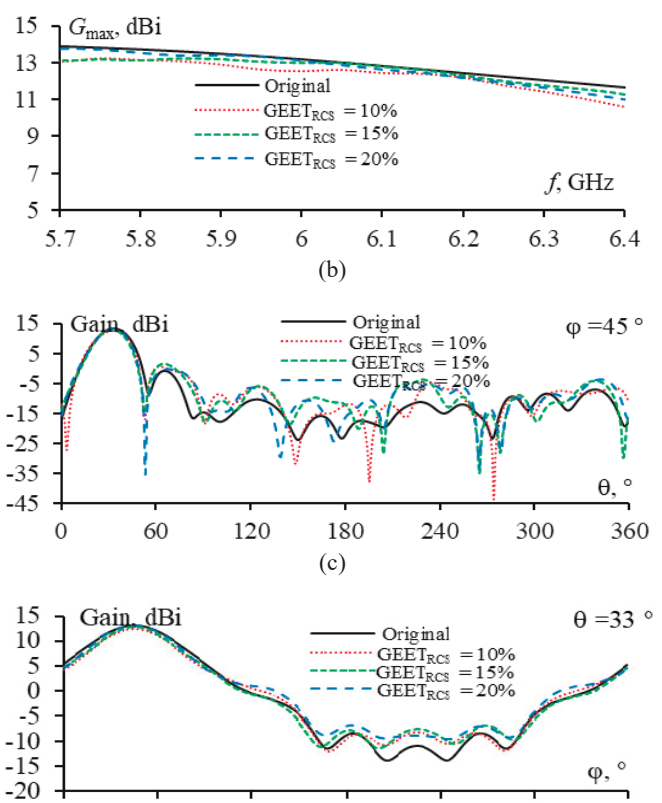


Fig. 6. Simulated $|s_{11}|$ (a), G_{max} (b), and RPs in the φ = 45° (c) and θ = 33° (d) planes at 6 GHz for the original and sparse antennas after L-RCS-OCGA

For each obtained sparse antenna, the MRCS was determined for two types of incident polarization, namely linear and circular polarization. In this study, the incident wave is expressed in the spherical coordinate system $\left(\hat{\boldsymbol{\theta}}, \hat{\boldsymbol{\varphi}}\right)$ according to the spatial phasor convention $e^{+j\mathbf{kr}}$. For linear polarization, the θ-polarized incident wave has its electric field vector oriented along $\hat{\boldsymbol{\theta}}$, and is expressed as

$$\mathbf{E}_{inc} = \hat{\boldsymbol{\theta}}\, e^{+j\mathbf{kr}}. \quad (1)$$

For circular polarization, the incident wave is expressed as

$$\mathbf{E}_{inc} = \frac{1}{\sqrt{2}}(\hat{\boldsymbol{\theta}} - j\hat{\boldsymbol{\varphi}})\, e^{+j\mathbf{kr}}, \quad (2)$$

which corresponds to a right-hand circularly polarized (RHCP) wave. An RHCP wave is one for which the electric field vector rotates clockwise when viewed in the direction of wave propagation.

As mentioned earlier, the TCR antenna exhibited its maximum MRCS at boresight (φ = 45° and θ ≈ 55°). For this reason, the boresight direction was selected as the main observation direction to analyze the MRCS over the operating frequency band.

For the θ-polarized (1) incident wave (Fig. 7), the sparse antennas exhibited a substantial MRCS reduction over the 5–8 GHz band in the boresight direction (Fig. 7a). The average MRCS reduction with respect to the original antenna was 8.74, 7.26, and 6.73 dB for GEET$_{RCS}$ = 10, 15, and 20%, respectively. This reduction was larger when GEET$_{RCS}$ was smaller, since a smaller GEET$_{RCS}$ resulted in a larger number of wires being additionally eliminated.

At 6 GHz in the φ = 45° plane (Fig. 7b), the MRCS reduction was clearly observed in the region of θ ≈ 30–80°, reaching up to 25 dB around θ = 75–80° for GEET$_{RCS}$ = 20%. A slight increase of MRCS, however, was observed in the region of θ = 12–24°. This effect may be attributed to a present limitation of the sparsification criterion, which considers only the magnitude of the current and does not yet account for its phase. The incorporation of phase information into the sparsification criterion is a direction that will be investigated in future work. In the θ = 55° plane at 6 GHz (Fig. 7c), the MRCS was reduced over all the considered directions, with the strongest reduction occurring around the boresight direction.

These results show that L-RCS-OCGA produces sparse antennas with a substantial MRCS reduction with respect to the original antenna for the θ-polarized incident wave.

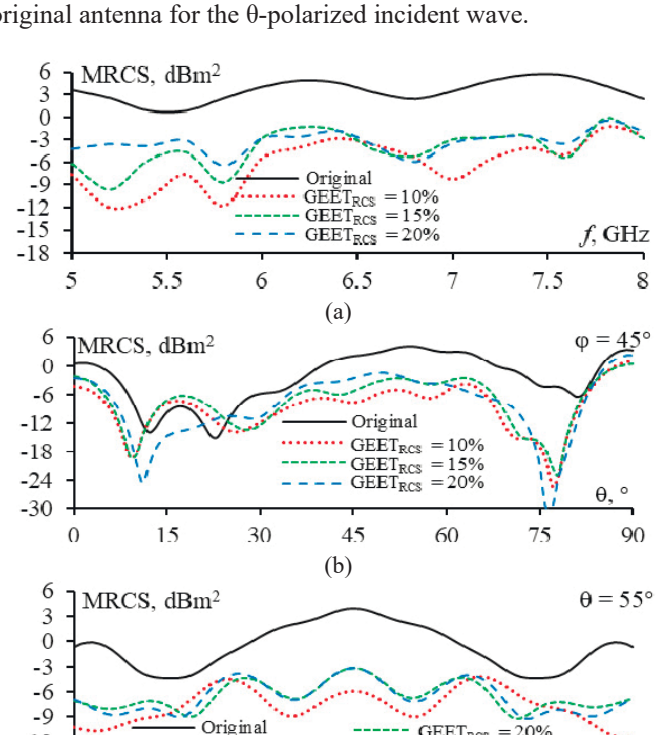
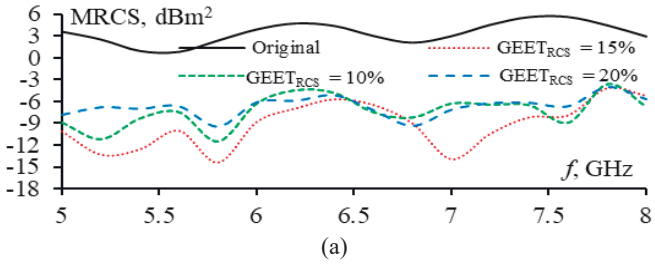


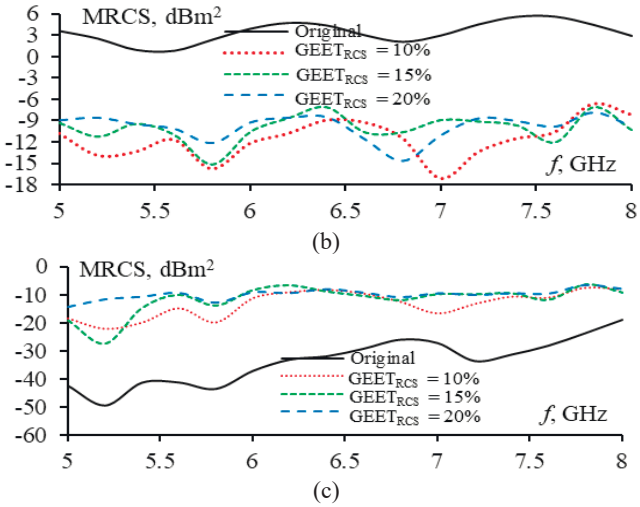
Fig. 7. Simulated MRCSs when the structures were excited by the plane wave with θ-pol over 5–8 GHz (a), in φ = 45° (b), θ = 55° (c) planes at 6 GHz for the original and sparse antennas

For the RHCP (2) incident wave, the sparse antennas also exhibited a substantial reduction of MRCS (Fig. 8). Over the 5-8 GHz band, the average reduction of the total MRCS with respect to the original was 12.12, 10.51, and 10.3 dB for GEET$_{RCS}$ = 10, 15, and 20%, respectively (Table 2). The reduction was even larger for the cross-polarization (cross-pol) component, reaching 14.75, 13.29, and 13.27 dB. The co-polarization (co-pol) component, on the other hand, showed an increase of 18.37, 20.17, and 20.57 dB. It should be noted that the co-pol MRCS of the original TCR antenna is inherently low. Although the increase of the co-pol component in the sparse antennas appears large when expressed in decibels, its absolute magnitude remains inherently small and does not dominate the cross-pol component.

At 6 GHz in the φ = 45° plane (Fig. 9a-c), the total and the cross-pol MRCS components were both reduced over most directions, with the strongest reduction occurring around the boresight direction (Fig. 9a and b). The co-pol component, in contrast, exhibited an increasing trend around the boresight direction (Fig. 9c), which was consistent with the increase of the co-pol component at boresight observed over the frequency band. In the θ = 55° plane at 6 GHz (Fig. 9d-f), similar trends were observed. The reduction of the total MRCS observed both over the frequency band and in the considered planes confirmed that L-RCS-OCGA reduced the total backscattered energy of the antenna for the RHCP incident wave, even though a portion of this energy was transferred to the co-pol component.



(a)



(b)

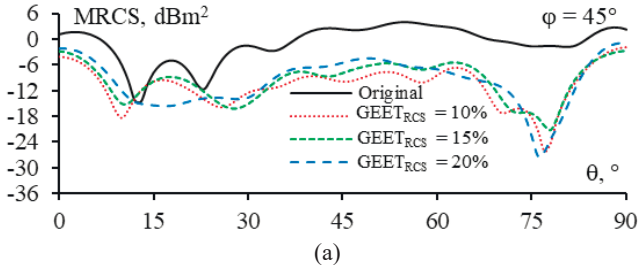
(c)

Fig. 8. Simulated total (a), cross-pol (b), and co-pol (c) MRCSs over 5-8 GHz when the structures were excited by the RHCP plane wave for the original and sparse antennas after L-RCS-OCGA

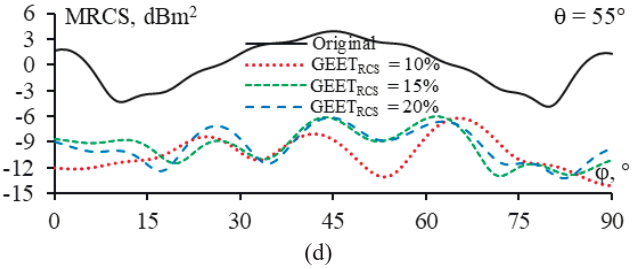
Table 2

Simulated G_{max} and average RCS change of the original and L-RCS-OCGA sparse antennas over 5–8 GHz

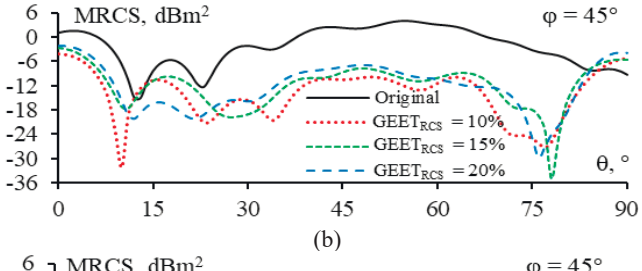
Structure	G_{max} at 6 GHz (dBi)	Avg. RCS reduction, θ-pol (dB)	Avg. RCS reduction, RHCP total (dB)	Avg. RCS reduction, RHCP cross-pol (dB)	Avg. RCS increase, RHCP co-pol (dB)	MRF
Original	13.18	-	-	-	-	-
GEET$_{RCS}$ = 10%	12.54	8.74	12.12	14.75	18.37	2.47
GEET$_{RCS}$ = 15%	13.00	7.26	10.51	13.29	20.17	2.25
GEET$_{RCS}$ = 20%	13.11	6.73	10.3	13.27	20.57	2.12



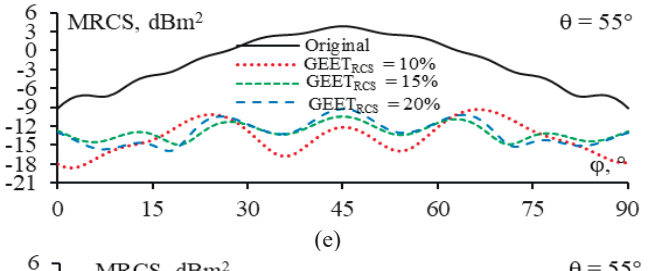
(a)



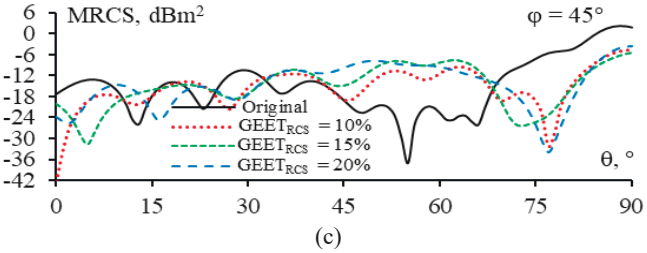
(d)



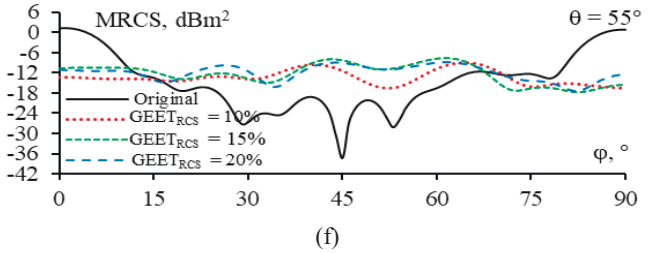
(b)



(e)



(c)



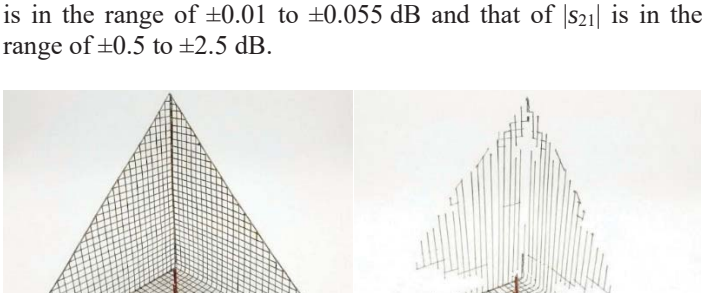
(f)

Fig. 9. Simulated total (a, d), cross-pol (b, e), and co-pol (c, f) MRCSs at 6 GHz when the structures were excited by the RHCP plane wave for the original and sparse antennas after L-RCS-OCGA

Thus, the application of L-RCS-OCGA to the TCR WG antenna simultaneously achieved three aims: a substantial mass reduction, a reduction of the MRCS for both θ-pol and RHCP incident waves, and a preservation of the basic radiation characteristics close to those of the original antenna. The results also revealed a trade-off between the level of RCS reduction and the preservation of the antenna characteristics. A smaller $GEET_{RCS}$ yields a larger RCS reduction but a more pronounced degradation of G_{max}, whereas a larger $GEET_{RCS}$ keeps the antenna characteristics closer to those of the original at the cost of a smaller RCS reduction. Among the considered cases, the sparse antenna with $GEET_{RCS}$ = 20% provided the best compromise, achieving MRF = 2.12, an average MRCS reduction of 6.73 dB for the θ-polarized incident wave and 10.3 dB for the total MRCS of the RHCP incident wave, while $|s_{11}|$ and G_{max} remained almost unchanged compared to those of the original antenna.

4 Experimental Results

To experimentally validate L-RCS-OCGA, two prototypes were fabricated, corresponding to the original TCR WG antenna and to the sparse antenna with $GEET_{RCS}$ = 20% (Fig. 10). Both prototypes were made of metallic wires, with dimensions matching those of the simulation model. All measurements were carried out in an anechoic chamber over the 5-8 GHz frequency band using a Micran R4M-18 vector network analyzer (10 MHz–20 GHz). For the MRCS measurements, two separate setups were used to generate the linearly and circularly polarized incident waves, and a metallic plate of known dimensions was used as the calibration reference for RCS measurement. According to the datasheet of the analyzer [27], the measurement error of $|s_{11}|$ is in the range of ±0.01 to ±0.055 dB and that of $|s_{21}|$ is in the range of ±0.5 to ±2.5 dB.



(a) (b)

Fig. 10. Prototypes of original (a)and sparse (b) TCR WG antennas

The measured and simulated $|s_{11}|$ for both the original and the sparse antennas are presented in Fig. 11a. For the original antenna, the measured resonant frequency was 6.06 GHz, compared with 6 GHz in the simulation, corresponding to a deviation of 60 MHz. This deviation may be attributed to fabrication tolerances and to the SMA connector, which was not included in the simulation model. Despite this small shift, the measured $|s_{11}|$ of the original antenna followed the simulated trend over the entire operating band.

For the sparse antenna with $GEET_{RCS}$ = 20%, the measured $|s_{11}|$ followed a trend similar to that of the original antenna. The deviation between the measured and simulated resonant frequencies of the sparse antenna was comparable to that of the original antenna, indicating that L-RCS-OCGA did not introduce any significant additional impedance mismatch. These results confirm that L-RCS-OCGA preserved the impedance matching of the antenna under practical fabrication conditions.

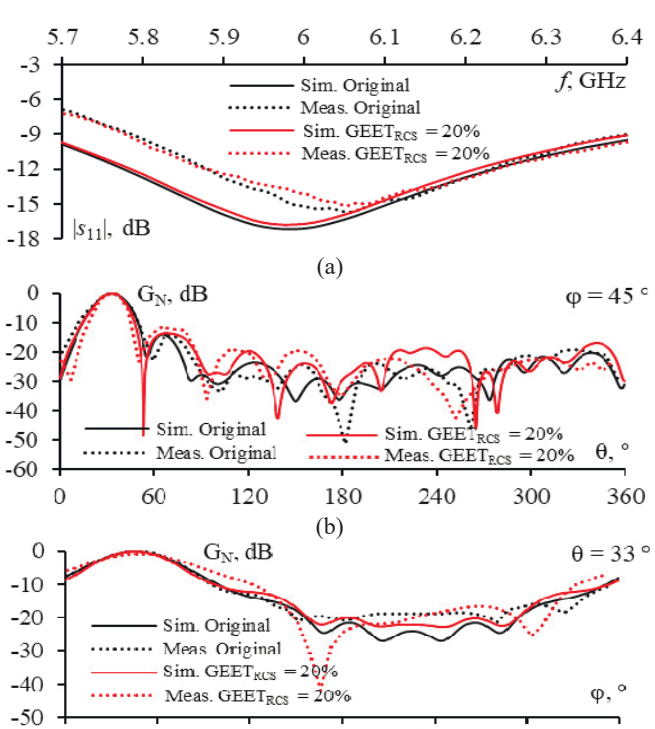


Fig. 11. Simulated and measured results of $|s_{11}|$ (a) and RPs in the φ = 45° (b), θ = 33° (c) planes at 6 GHz for the original and sparse antennas

The normalized RPs (G_N) in the φ = 45° and θ = 33° planes are presented in Fig. 11b and c. For the original antenna, the measured main beam agreed well with the simulated one in terms of both direction and beam width. The deviations in the SLL between measurement and simulation may be attributed to fabrication tolerances, angular alignment errors during the measurement, and the routing of the measurement cables near the antenna structure. For the sparse antenna with $GEET_{RCS}$ = 20%, the measured main beam closely matched the simulated and measured main beam of the original antenna, indicating that L-RCS-OCGA preserved the main radiation characteristics of the antenna. The increasing trend of the measured SLL with respect to the original one was consistent with the observations from the simulations discussed in Section 3.

Fig. 12a presents the MRCS at the boresight direction over the 5–8 GHz frequency band under θ-polarized incidence. The measured MRCS of the original antenna generally followed the simulated trend, with good agreement in the 5.5–8 GHz range. Over 5–5.5 GHz, the deviation between measurement and simulation was larger, reaching approximately 2.7 dB at 5.2 GHz, mainly due to angular alignment errors of the sample and the measurement antenna in the anechoic chamber. For the sparse antenna, the measured MRCS remained noticeably lower than that of the original antenna over the entire frequency band. The average measured MRCS reduction was 8.16 dB, and the simulated value was 6.73 dB. Both values confirm the effectiveness of L-RCS-OCGA in reducing the MRCS when the wire-elimination criterion is applied under practical fabrication conditions.

The MRCS at 6 GHz in the φ = 45° and θ = 55° planes under θ-polarized incidence is presented in Fig. 12b and c, respectively. In both planes, the measured MRCS of the sparse antenna was lower than that of the original antenna in most directions, with the strongest reduction occurring around the boresight direction. The experimental results confirm the trend of RCS reduction along the boresight direction observed in the simulations.

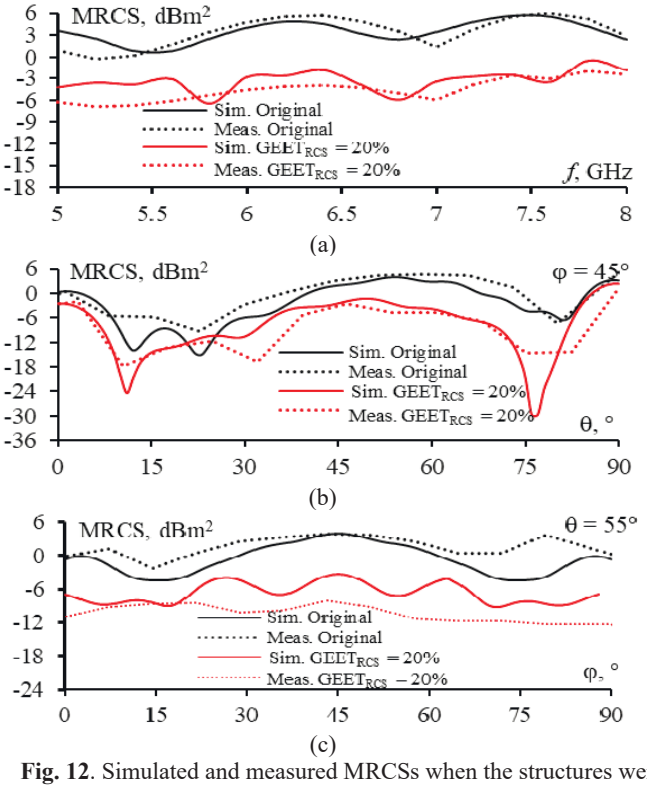


Fig. 12. Simulated and measured MRCSs when the structures were excited by plane wave with θ-pol over 5–8 GHz (a) in φ = 45° (b) and θ = 55° (c) planes at 6 GHz

When the structures were excited by an RHCP incident wave, the measured MRCSs of the cross-pol and co-pol components in the φ = 45° and θ = 55° planes are presented in Fig. 13. For the cross-pol component (Fig. 13a and c), the measured results showed a substantial MRCS reduction in most directions, particularly around the boresight direction, in agreement with the trend obtained in the simulations. In the θ = 55° plane (Fig. 13c), however, some deviations between measurement and simulation were observed. Specifically, the measured MRCS of the original antenna was about 6 dB higher than the simulated one in the angular range of φ = 65-80°. These deviations mainly originated from angular alignment errors of the prototypes during the measurement. Despite these deviations between simulation and measurement, the direct comparison between the measured results of the original and the sparse antennas still clearly demonstrates the MRCS reduction provided by the L-RCS-OCGA procedure. For the co-pol component (Fig. 13b and d), both the simulation and the measurement showed an increase of the MRCS around the boresight direction.

Overall, the experimental results demonstrate a strong correlation with the simulation results, although some discrepancies were observed at certain frequencies and angles. These discrepancies do not negate the effectiveness of the L-RCS-OCGA procedure under practical fabrication conditions, which successfully achieves all three objectives: weight reduction, preservation of fundamental radiation characteristics, and reduction of the antenna MRCS.

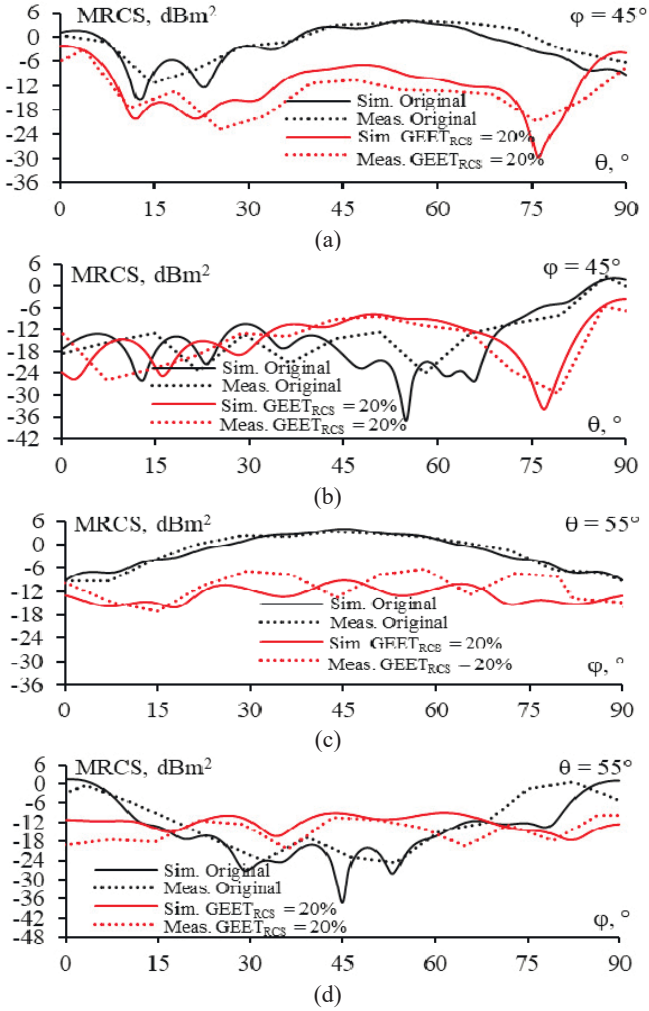


Fig. 13. Simulated and measured cross-pol (a, c) and co-pol (b, d) MRCSs when the original and sparse antennas were excited by the RHCP plane wave at 6 GHz

5. Discussion

The L-RCS-OCGA demonstrates its effectiveness in simultaneously achieving all three objectives: mass reduction, RCS reduction, and preservation of the fundamental radiation characteristics at levels comparable to those of the original antenna. The reduction of the total MRCS confirms that the sparse structure obtained by L-RCS-OCGA achieved a genuine decrease in the total backscattered energy, rather than merely redistributing a portion of that energy to the co-polarization component. These results are achieved entirely through wire removal, without the integration of any auxiliary structures. Furthermore, fabrication does not require specialized materials or complex processing steps, making L-RCS-OCGA well suited to platforms with stringent payload constraints. Within L-RCS-OCGA, the reconnection mechanism also plays an important role in ensuring fabrication feasibility without compromising the previously achieved RCS reduction.

In the existing OCGA modifications, the reconnection mechanism is designed primarily to maintain mass reduction or to

preserve the radiation characteristics, without accounting for the contribution of the restored wires to the scattered field. Specifically, NCOCGA [16] selects wires to be restored based solely on the shortest-path criterion, without controlling their current magnitude, which may result in the inadvertent restoration of wires that have little influence on the radiation field or contribute strongly to the scattered field. MCOCGA [17] gives priority to the restoration of wires with the largest radiation currents along a path. However, as noted in [18], this algorithm may inadvertently restore wires that already belong to the main structure and does not guarantee that all free-wire components are reconnected. L-RCS-OCGA addresses these limitations and, to the best of the authors' knowledge, is the first approach in the OCGA family to incorporate scattering awareness into both the wire-elimination and reconnection steps.

Nevertheless, the wire-elimination criterion adopted in L-RCS-OCGA considers only the magnitude of the current and does not yet account for phase information. This limitation is believed to be responsible for the localized increase in MRCS observed at certain off-boresight directions in the simulation results. The incorporation of phase information into the sparsification criterion, therefore, represents a direct avenue for further development. In addition, extending the validation of L-RCS-OCGA to WG antenna structures of greater complexity will allow a more comprehensive assessment of the applicability limits of the approach and further optimization of the trade-off among mass, RCS, and radiation characteristics.

6. Conclusions

This study has proposed L-RCS-OCGA for WG antennas to simultaneously reduce both their mass and RCS while preserving the fundamental radiation characteristics. The approach was validated on a TCR WG antenna operating at 6 GHz, with the monostatic RCS examined over the 5-8 GHz band for both theta-polarized and RHCP incident waves. At $GEET_{RCS}$ = 20%, the representative sparse antenna achieved MRF = 2.12, with an average MRCS reduction at boresight of 6.73 dB (simulated) and 8.16 dB (measured) for theta-polarized incidence, and 10.3 dB (simulated) for the total RHCP component. The $|s_{11}|$ and G_{max} of the sparse antenna remained close to those of the original. The reduction of the total MRCS confirms that the sparse structure genuinely decreases the backscattered energy. Future development will focus on incorporating the phase information of the current into the sparsification criterion and on extending the validation to WG antenna structures of greater complexity.

Funding: This research was funded by the Ministry of Science and Higher Education of the Russian Federation project FEWM-2024-0005.

References

[1] S. Gundapaneni, G. S. N. Raju, and A. S. D. Pendurthi, "Inverted T-Shaped Antenna for 2.45 GHz ISM Band Wearable Applications," *Iran. J. Sci. Technol. Trans. Electr. Eng.*, vol. 47, no. 4, pp. 1177-1186, Dec. 2023. doi: 10.1007/s40998-023-00596-8.

[2] V. Rajavel and D. Ghoshal, "AMC-Based Low-Profile Dual-Band Slotted Patch Antenna for IoT Devices in the Healthcare System," *Iran. J. Sci. Technol. Trans. Electr. Eng.*, vol. 47, no. 2, pp. 437-450, Jun. 2023. doi: 10.1007/s40998-022-00581-7.

[3] N. Gupta, J. Saxena, and K. S. Bhatia, "Design of Metamaterial-Loaded Rectangular Patch Antenna for Satellite Communication Applications," *Iran. J. Sci. Technol. Trans. Electr. Eng.*, vol. 43, no. S1, pp. 39-49, Dec. 2019. doi: 10.1007/s40998-019-00213-7.

[4] M. Liang, C. Shemelya, E. MacDonald, R. Wicker, and H. Xin, "3-D Printed Microwave Patch Antenna via Fused Deposition Method and Ultrasonic Wire Mesh Embedding Technique," *IEEE Antennas Wireless Propag. Lett.*, vol. 14, pp. 1346-1349, 2015. doi: 10.1109/LAWP.2015.2405054.

[5] Y. Shi, X. F. Zhang, Z. K. Meng, and L. Li, "Design of Low-RCS Antenna Using Antenna Array," *IEEE Trans. Antennas Propag.*, vol. 67, no. 10, pp. 6484-6493, Oct. 2019. doi: 10.1109/TAP.2019.2925180.

[6] Y. Azizi, M. Soleimani, S. H. Sedighy, and L. Matekovits, "Low-Cost, Low-Profile Wide-Band Radar Cross Section Reduction Using Dual-Concentric Phase-Gradient Modulated Surface," *Electronics*, vol. 10, no. 13, p. 1552, Jun. 2021. doi: 10.3390/electronics10131552.

[7] T. Zhang, J. Ren, Y. Yang, X. Pang, and Q. Zheng, "Ultra-wideband Low-RCS and gain-enhanced phase gradient metasurface-based antenna using characteristic mode analysis," *AEU - Int. J. Electron. Commun.*, vol. 183, p. 155370, Aug. 2024. doi: 10.1016/j.aeue.2024.155370.

[8] Z. Tian *et al.*, "Broadband low-profile and Low-RCS circular polarization metasurface antenna based on hybrid mechanism with characteristic mode analysis," *AEU - Int. J. Electron. Commun.*, vol. 202, p. 156043, Jan. 2025. doi: 10.1016/j.aeue.2025.156043.

[9] H. Umair *et al.*, "Tilted Beam Fabry-Perot Antenna with Enhanced Gain and Broadband Low Backscattering," *Electronics*, vol. 10, no. 3, p. 267, Jan. 2021. doi: 10.3390/electronics10030267.

[10] S. A. Harooni, M. Naser-Moghadasi, B. Ghalamkari, and M. Khatir, "Wideband RCS reduction in microstrip antennas using integrated artificial magnetic conductors and frequency-selective surface," *AEU - Int. J. Electron. Commun.*, vol. 205, p. 156135, Mar. 2026. doi: 10.1016/j.aeue.2025.156135.

[11] G. Saxena, Y. K. Awasthi, and P. Jain, "Design of metasurface absorber for low RCS and high isolation MIMO antenna for radio location & navigation," *AEU - Int. J. Electron. Commun.*, vol. 133, p. 153680, May 2021. doi: 10.1016/j.aeue.2021.153680.

[12] J. Han, D. Jia, B. Du, G. Han, Y. Jia, and Z. Zhao, "Design of Broadband Low-RCS Array Antennas Based on Characteristic Mode Cancellation," *Electronics*, vol. 12, no. 7, p. 1536, Mar. 2023. doi: 10.3390/electronics12071536.

[13] Y. Liu, B. Du, and D. Jia, "Design of Broad-Angle Low-RCS Microstrip Antenna for Dual-Polarization Using Characteristic Mode Analysis," *Electronics*, vol. 14, no. 11, p. 2121, May 2025. doi: 10.3390/electronics14112121.

[14] M. U. Ullah *et al.*, "A progression in the techniques of reducing RCS for the targets," *Alexandria Eng. J.*, vol. 100, pp. 153–169, Aug. 2024. doi: 10.1016/j.aej.2024.05.001.

[15] A. F. Alhaj Hasan, M. T. Nguyen, and T. R. Gazizov, "Modelling and designing wire-grid sparse antennas using MoM-based approaches for enhanced performance and reduced cost," *Mikrotalasna Rev.*, vol. 29, no. 2, pp. 83–94, Dec. 2023. doi: 10.18485/mtts_mr.2023.29.2.10.

[16] A. F. Alhaj Hasan, M. T. Nguyen, and T. R. Gazizov, "Novel MoM-Based Approaches for Generating Wire-Grid Sparse Antenna Structures," in *Proc. IEEE 24th Int. Conf. Young Professionals in Electron Devices Materials (EDM)*, 2023, pp. 570–576. doi: 10.1109/EDM58354.2023.10225219.

[17] M. T. Nguyen, A. F. Alhaj Hasan, and T. R. Gazizov, "Generating sparse wire-grid antennas using maximum current-based optimal current grid approximation," *IEEE Open J. Antennas Propag.*, vol. 6, pp. 112–121, 2025. doi: 10.1109/OJAP.2025.3543559.

[18] T. P. Dang and T. R. Gazizov, "Improving the optimal current grid approximation for sparse scattering structures," *Radiotekhnika*, no. 9, pp. 181–192, 2025. doi: 10.18127/j00338486-202509-20.

[19] M. T. Nguyen and T. R. Gazizov, "Design of monopole antennas with various grounds for 2.4 GHz applications," *AEU - Int. J. Electron. Commun.*, vol. 202, p. 156050, Jan. 2025. doi: 10.1016/j.aeue.2025.156050.

[20] R. F. Harrington, "Matrix methods for field problems," *Proc. IEEE*, vol. 55, no. 2, pp. 136–149, Feb. 1967. doi: 10.1109/PROC.1967.5432.

[21] N. Inagaki, "Three-dimensional corner reflector antenna," *IEEE Trans. Antennas Propag.*, vol. 22, no. 4, pp. 580–582, Jul. 1974. doi: 10.1109/TAP.1974.1140853.

[22] D. Dobričić, "Shortened 3D corner reflector antenna," QSL.net, 2012. [Online]. Available: https://www.qsl.net/yu1aw/ANT_VHF/Shortened%203D%20Corner%20Reflector%20Antenna.pdf

[23] E. W. Dijkstra, "A note on two problems in connexion with graphs," *Numer. Math.*, vol. 1, no. 1, pp. 269–271, Dec. 1959. doi: 10.1007/BF01386390.

[24] D. G. Michelson and E. Jull, "Depolarizing Trihedral Corner Reflectors for Radar Navigation and Remote Sensing," *IEEE Trans. Antennas Propag.*, vol. 43, no. 5, pp. 513–518, May 1995. doi: 10.1109/8.384196.

[25] C. Gennarelli, G. Pelosi, and G. Riccio, "Physical optics analysis of the field backscattered by a depolarising trihedral corner reflector," *IEE Proc. - Microw. Antennas Propag.*, vol. 145, no. 3, pp. 213–218, Jun. 1998. doi: 10.1049/ip-map:19981821.

[26] I. Hänninen, M. Pitkonen, K. I. Nikoskinen, and J. Sarvas, "Method of Moments Analysis of the Backscattering Properties of a Corrugated Trihedral Corner Reflector," *IEEE Trans. Antennas Propag.*, vol. 54, no. 4, pp. 1167–1173, Apr. 2006. doi: 10.1109/TAP.2006.1614173.

[27] *R4M Vector Network Analyzers*, Micran, Tomsk, Russia, 2021. [Online]. Available: https://micran.com/upload/iblock/ffd/R4M%20vector%20network%20analyzers.pdf

СОЗДАНИЕ РАЗРЕЖЕННЫХ ПРОВОДНО-СЕТОчНЫХ АНТЕНН С УМЕНЬШЕННОЙ ЭПР, ИСПОЛЬЗУц НОВУЮ МОДИФИКАЦИЮ АППРОКСИМАЦИИ ОПТИМАЛЬНОЙ ТОКОВОЙ СЕТКОЙ

Суан Ба Чинь, *Томский государственный университет систем управления и радиоэлектроники (ТУСУР), Томск, Россия,* ***xuanba6420@gmail.com***

Газизов Тальгат Рашитович, *Томский государственный университет систем управления и радиоэлектроники (ТУСУР), Томск, Россия,* ***talgat.r.gazizov@tusur.ru***

Аннотация

Одновременное снижение массы и эффективной площади рассеяния (ЭПР) антенны является важной и актуальной задачей проектирования в современных исследованиях. В данной работе предлагается аппроксимация оптимальной токовой сеткой с уменьшением ЭПР (У-ЭПР-АОТС), направленная на одновременное снижение как массы, так и ЭПР антенны при сохранении ее основных характеристик излучения. Предлагаемый подход разреживает структуру антенны из проводной сетки (ПС) удалением тех проводов, которые вносят незначительный вклад в поле излучения, но при этом сильно влияют на поле рассеяния. После этого восстанавливается связность между несоединенными структурами путем восстановления удаленных проводов, обладающих наименьшим вкладом в рассеянное поле. Данный подход представляет собой модификацию, в которой впервые в семействе АОТС учитываются характеристики рассеяния на этапах как удаления проводов, так и восстановления связности структуры. Эффективность У-ЭПР-АОТС подтверждена результатами моделирования и измерения на треугольной трехгранной уголковой рефлекторной антенне из ПС, работающей на частоте 6 ГГц. Моностатическая ЭПР (МЭПР) исследовалась в диапазоне частот 5-8 ГГц для падающих волн с -поляризацией и правой круговой поляризацией (ПКП). Разреженная антенна оказалась в 2,12 раза легче исходной. При этом среднее снижение МЭПР в направлении главного луча составило 6,73 дБ (при моделировании) и 8,16 дБ (при измерении) для -поляризации, а также 10,3 дБ (при моделировании) для полной компоненты волны с ПКП. В то же время основные характеристики излучения при этом остались близки к исходной антенне. Таким образом, У-ЭПР-АОТС обеспечивает эффективное одновременное снижение массы и ЭПР антенны, что делает его особенно перспективным для применения на платформах со строгими ограничениями по полезной нагрузке.

Ключевые слова: *аппроксимация оптимальной токовой сеткой, метод моментов, проводная сетка, разреженная антенна, эффективная площадь рассеяния.*

Литература

1. *Gundapaneni S., Raju G. S. N., Pendurthi A. S. D.* Inverted T-Shaped Antenna for 2.45 GHz ISM Band Wearable Applications // Iran Journal of Science and Technology, Transactions of Electrical Engineering. 2023. Vol. 47, no. 4. P. 1177-1186. doi: 10.1007/s40998-023-00596-8.

2. *Rajavel V., Ghoshal D.* AMC-Based Low-Profile Dual-Band Slotted Patch Antenna for IoT Devices in the Healthcare System // Iran Journal of Science and Technology, Transactions of Electrical Engineering. 2023. Vol. 47, no. 2. P. 437-450. doi: 10.1007/s40998-022-00581-7.

3. *Gupta N., Saxena J., Bhatia K. S., Khah M. M.* Design of Metamaterial-Loaded Rectangular Patch Antenna for Satellite Communication Applications // Iran Journal of Science and Technology, Transactions of Electrical Engineering. 2019. Vol. 43, no. Suppl 1. P. 39-49. doi: 10.1007/s40998-019-00213-7.

4. *Liang M., Shemelya C., MacDonald E., Wicker R., Xin H.* 3-D Printed Microwave Patch Antenna via Fused Deposition Method and Ultrasonic Wire Mesh Embedding Technique // IEEE Antennas and Wireless Propagation Letters. 2015. Vol. 14. P. 1346-1349. doi: 10.1109/LAWP.2015.2405054.

5. *Shi Y., Zhang X. F., Meng Z. K., Li L.* Design of Low-RCS Antenna Using Antenna Array // IEEE Transactions on Antennas and Propagation. 2019. Vol. 67, no. 10. P. 6484-6493. doi: 10.1109/TAP.2019.2925180.
6. *Azizi Y., Soleimani M., Sedighy S. H., Matekovits L.* Low-Cost, Low-Profile Wide-Band Radar Cross Section Reduction Using Dual-Concentric Phase-Gradient Modulated Surface // Electronics. 2021. Vol. 10, no. 13. Art. no. 1552. doi: 10.3390/electronics10131552.
7. *Zhang T., Ren J., Yang Y., Pang X., Zheng Q.* Ultra-wideband Low-RCS and gain-enhanced phase gradient metasurface-based antenna using characteristic mode analysis // AEU – International Journal of Electronics and Communications. 2024. Vol. 183. Art. no. 155370. doi: 10.1016/j.aeue.2024.155370.
8. *Tian Z., Yang L., Cheng Z., Cai B., Cheng Y., Luo H., Li X.* Broadband low-profile and Low-RCS circular polarization metasurface antenna based on hybrid mechanism with characteristic mode analysis // AEU – International Journal of Electronics and Communications. 2025. Vol. 202. Art. no. 156043. doi: 10.1016/j.aeue.2025.156043.
9. *Umair H., Latef T. B. A., Yamada Y., Mahadi W. N. L. B. W., Othman M., Kamardin K., Hussein M. I., Najam A. I.* Tilted Beam Fabry-Perot Antenna with Enhanced Gain and Broadband Low Backscattering // Electronics. 2021. Vol. 10, no. 3. Art. no. 267. doi: 10.3390/electronics10030267.
10. *Harooni S. A., Naser-Moghadasi M., Ghalamkari B., Khatir M.* Wideband RCS reduction in microstrip antennas using integrated artificial magnetic conductors and frequency-selective surface // AEU – International Journal of Electronics and Communications. 2026. Vol. 205. Art. no. 156135. doi: 10.1016/j.aeue.2025.156135.
11. *Saxena G., Awasthi Y. K., Jain P.* Design of metasurface absorber for low RCS and high isolation MIMO antenna for radio location & navigation // AEU – International Journal of Electronics and Communications. 2021. Vol. 133. Art. no. 153680. doi: 10.1016/j.aeue.2021.153680.
12. *Han J., Jia D., Du B., Han G., Jia Y., Zhao Z.* Design of Broadband Low-RCS Array Antennas Based on Characteristic Mode Cancellation // Electronics. 2023. Vol. 12, no. 7. Art. no. 1536. doi: 10.3390/electronics12071536.
13. *Liu Y., Du B., Jia D.* Design of Broad-Angle Low-RCS Microstrip Antenna for Dual-Polarization Using Characteristic Mode Analysis // Electronics. 2025. Vol. 14, no. 11. Art. no. 2121. doi: 10.3390/electronics14112121.
14. *Ullah M. U., Latef T. B. A., Othman M., Hussein M. I., Alkhoori H. M., Yamada Y., Kamardin K., Khalid R.* A progression in the techniques of reducing RCS for the targets // Alexandria Engineering Journal. 2024. Vol. 100. P. 153-169. doi: 10.1016/j.aej.2024.05.001.
15. *Alhaj Hasan A. F., Nguyen M. T., Gazizov T. R.* Modelling and designing wire-grid sparse antennas using MoM-based approaches for enhanced performance and reduced cost // Mikrotalasna Revija. 2023. Vol. 29, no. 2. P. 83-94. doi: 10.18485/mtts_mr.2023.29.2.10.
16. *Alhaj Hasan A. F., Nguyen M. T., Gazizov T. R.* Novel MoM-Based Approaches for Generating Wire-Grid Sparse Antenna Structures // Proceedings of 2023 IEEE 24th International Conference of Young Professionals in Electron Devices and Materials (EDM). 2023. P. 570-576. doi: 10.1109/EDM58354.2023.10225219.
17. *Nguyen M. T., Alhaj Hasan A. F., Gazizov T. R.* Generating sparse wire-grid antennas using maximum current-based optimal current grid approximation // IEEE Open Journal of Antennas and Propagation. 2025. Vol. 6. P. 112-121. doi: 10.1109/OJAP.2025.3543559.
18. *Dang T. P., Gazizov T. R.* Improving the optimal current grid approximation for sparse scattering structures // Radiotekhnika. 2025. No. 9. P. 181-192. doi: 10.18127/j00338486-202509-20.
19. *Nguyen M. T., Gazizov T. R.* Design of monopole antennas with various grounds for 2.4 GHz applications // AEU - International Journal of Electronics and Communications. 2025. Vol. 202. Art. no. 156050. doi: 10.1016/j.aeue.2025.156050.
20. *Harrington R. F.* Matrix methods for field problems // Proceedings of the IEEE. 1967. Vol. 55, no. 2. P. 136-149. doi: 10.1109/PROC.1967.5432.
21. *Inagaki N.* Three-dimensional corner reflector antenna // IEEE Transactions on Antennas and Propagation. 1974. Vol. 22, no. 4. P. 580-582. doi: 10.1109/TAP.1974.1140853.
22. *Dobricic D.* Shortened 3D corner reflector antenna. 2012. [Электронный ресурс]. URL: https://www.qsl.net/yu1aw/ANT_VHF/Shortened%203D%20Corner%20Reflector%20Antenna.pdf (дата обращения: 06.04.2026).
23. *Dijkstra E. W.* A note on two problems in connexion with graphs // Numerische Mathematik. 1959. Vol. 1, no. 1. P. 269-271. doi: 10.1007/BF01386390.
24. *Michelson D. G., Jull E.* Depolarizing Trihedral Corner Reflectors for Radar Navigation and Remote Sensing // IEEE Transactions on Antennas and Propagation. 1995. Vol. 43, no. 5. P. 513-518. doi: 10.1109/8.384196.
25. *Gennarelli C., Pelosi G., Riccio G.* Physical optics analysis of the field backscattered by a depolarising trihedral corner reflector // IEE Proceedings – Microwaves, Antennas and Propagation. 1998. Vol. 145, no. 3. P. 213-218. doi: 10.1049/ip-map:19981821.
26. *Hanninen I., Pitkonen M., Nikoskinen K. I., Sarvas J.* Method of Moments Analysis of the Backscattering Properties of a Corrugated Trihedral Corner Reflector // IEEE Transactions on Antennas and Propagation. 2006. Vol. 54, no. 4. P. 1167-1173. doi: 10.1109/TAP.2006.1614173.
27. R4M vector network analyzers / Micran. Tomsk, Russia, 2021. [Электронный ресурс]. URL: https://micran.com/upload/iblock/ffd/R4M%20vector%20network%20analyzers.pdf (дата обращения: 02.05.2026).

Информация об авторах:
Суан Ба Чинь, аспирант, *ТУСУР, Томск, Россия. ORCID: 0009-0000-5711-5878*
Газизов Тальгат Рашитович, *д.т.н., проф., заведующий каф., ТУСУР, Томск, Россия. ORCID: 0009-0000-6287-1117*